AAS 13-484

PASSIVE SORTING OF ASTEROID MATERIAL USING SOLAR RADIATION PRESSURE

D. García Yárnoz,[*] J. P. Sánchez Cuartielles,[†] and C. R. McInnes [‡]

Understanding dust dynamics in asteroid environments is key for future science missions to asteroids and, in the long-term, also for asteroid exploitation. This paper proposes a novel way of manipulating asteroid material by means of solar radiation pressure (SRP). We envisage a method for passively sorting material as a function of its grain size where SRP is used as a passive in-situ 'mass spectrometer'. The analysis shows that this novel method allows an effective sorting of regolith material. This has immediate applications for sample return, and in-situ resource utilisation to separate different regolith particle sizes

INTRODUCTION

Asteroids have lately become prime targets for space exploration missions. This interest is justified as asteroids are among the least evolved bodies in the Solar System and they can provide a better understanding of its formation from the solar nebula. Under NASA's flexible path plan,[1] asteroids have also become one of the feasible "planetary" surfaces to be visited by crewed missions, with the benefit of not requiring the capability to land and take-off from a deep gravity well. In addition, they may well be the most affordable source of in-situ resources to underpin future space exploration ventures.

Considerable efforts have been made in the study of the perturbing forces and space environment around cometary and asteroid bodies.[2, 3] These forces and harsh environments need to be considered and will have direct implications for the operations of spacecraft around and on small bodies. However, they may also represent an opportunity, if engineered for our own benefit, to device new types of highly non-keplerian trajectories and novel resources exploitation methods.

Recent asteroid observations (e.g., Itokawa) indicate that all observed NEOs, including very small objects, are not bare lumps of rock.[4] A very fine layer of regolith material has a ubiquitous presence in all asteroid surfaces. The presence of this fine dust, coupled with the weak and irregular gravitational environments, increases the risk of triggering transient dust atmospheres during asteroid operations that can potentially degrade instrumentation, damage mechanisms and reduce visibility and communications. An analysis of the dynamical behaviour of asteroid dust under solar radiation pressure (SRP) allows the definition of a series of asteroid-spacecraft-Sun configurations that minimise the risk of transient dust atmospheres around the asteroid during operations.

[*] PhD Researcher, Advanced Space Concepts Laboratory, Dept. of Mechanical and Aerospace Engineering, University of Strathclyde, Glasgow G1 1XQ, UK.
[†] Research Fellow, Advanced Space Concepts Laboratory.
[‡] Director, Advanced Space Concepts Laboratory.

Additionally, this paper proposes a novel method for sorting asteroid material, exploiting the dynamical interaction of dust contained in the asteroid regolith and solar radiation pressure. This has immediate applications for a possible sample return mission to an asteroid, such as allowing in-situ separation of different regolith sizes, or separation of different materials based on their density. Future asteroid engineering and mining endeavours would benefit from this sorting technique, analogous to winnowing on Earth, where solar radiation pressure is used as a passive in-situ 'mass spectrometer'.

Exploiting the Forces Affecting Ejected Dust in the Asteroid Environment

Depending on the size of the asteroid and its spin state, the effective ambient gravitational acceleration experienced by dust grains on small bodies can range from micro-gravity to milli-gravity[2]. Under such conditions, the SRP perturbation becomes the largest non-gravitational force affecting grains that have been lifted from the asteroid's surface, either naturally by micrometeoroid impacts or electrostatic forces, or artificially by mechanical means. Dust grains with a large enough area-to-mass ratio can escape from the asteroid,[5] while those with smaller area-to-mass ratios will stay bounded, but their trajectories will also be perturbed, even when ejected with the same low initial velocity. Based on this effect of differential SRP influence on dust grains, we therefore envisage a method for passively sorting asteroid material as a function of grain size. The method consists of one surface element that collects loose material directly from the asteroid and expels it at small velocities at some angle to the surface, and one or several "collectors" that capture particles as they fall back to the surface.

In the following sections we will put forward simplified equations describing the trajectories of dust particles around an asteroid considering the third body perturbation of the Sun and the solar radiation pressure perturbation. In order to achieve a better understanding of the different regimes of the orbiting dust, a simple analytical formulation is explained and applied to the problem. Both the analytical approximation and numerical propagations prove useful in studying the behaviour of the dust particles and important conclusions can be drawn from the analysis regarding the engineering of forces around asteroids.

THE PHOTO-GRAVITATIONAL RESTRICTED 3-BODY PROBLEM

The problem to be tackled can be modelled, in a first approximation, by the well-known photo-gravitational circular restricted three body problem[6-8] applied to a spherical asteroid. Assuming dust grains of constant density, the ratio of SRP perturbation with respect to the gravitational attraction of the Sun can be represented with the lightness number β:

$$\beta = \frac{3LQ}{16\pi c \mu_S r \rho} \tag{1}$$

where L is the solar luminosity, Q the solar radiation pressure coefficient, which depends on the material properties, c is the speed of light, μ_S is the gravitational constant of the Sun, r is the equivalent particle radius, and ρ is the density of the particle. This parameter will prove useful to describe the different orbiting regimes of particles around an asteroid. Clearly, β is proportional to the area-to-mass ratio, so for a fixed density, β decreases with the particle radius. Therefore, for small dust grains, SRP can provide a significant perturbing force.

We consider an asteroid in a circular orbit of distance d around the Sun. Defining a co-rotating frame centred on the barycentre of the system and with the x-axis pointing towards the asteroid (see Figure 1), the motion of a particle can be described by the following set of differential equations:

$$\begin{cases} \ddot{x} - 2\Omega_R \dot{y} = \Omega_R{}^2 \left(x - \dfrac{(1-\mu)(1-\beta)(x+\mu)}{\left((x+\mu)^2 + y^2 + z^2\right)^{3/2}} - \dfrac{\mu(x+\mu-1)}{\left((x+\mu-1)^2 + y^2 + z^2\right)^{3/2}} \right) \\ \ddot{y} + 2\Omega_R \dot{x} = \Omega_R{}^2 \left(y - \dfrac{(1-\mu)(1-\beta)y}{\left((x+\mu)^2 + y^2 + z^2\right)^{3/2}} - \dfrac{\mu y}{\left((x+\mu-1)^2 + y^2 + z^2\right)^{3/2}} \right) \\ \ddot{z} = \Omega_R{}^2 \left(- \dfrac{(1-\mu)(1-\beta)z}{\left((x+\mu)^2 + y^2 + z^2\right)^{3/2}} - \dfrac{\mu z}{\left((x+\mu-1)^2 + y^2 + z^2\right)^{3/2}} \right) \end{cases} \quad (2)$$

$$\mu = \frac{\mu_A}{\mu_A + \mu_S}; \quad \Omega_R = \sqrt{\frac{\mu_A + \mu_S}{d^3}} \quad (3)$$

where distances have been normalized with respect to d, μ_S and μ_A are the gravitational constants of the Sun and the asteroid respectively, and Ω_R is the frequency of rotation of the two bodies (and the frame) around the barycentre. Higher order gravitational perturbations of the asteroid, which can be of great importance for irregularly shaped asteroids, are not taken into account at this stage of the investigation. Eclipses have also been ignored.

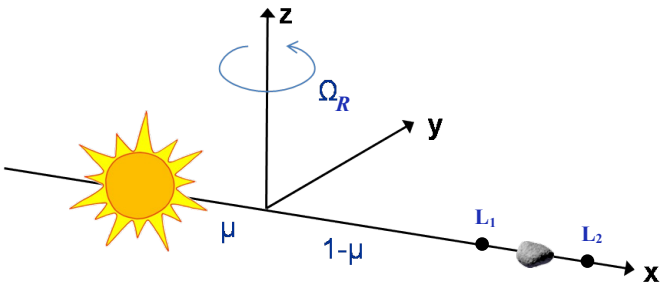

Figure 1. Schematic representation of the co-rotating frame centred in the barycentre of the Sun-asteroid system.

This system of equations has an integral of motion $C = -2E = 2U-2T$, where U and T are the potential and kinetic energy, which can be expressed as:

$$U = \frac{1}{2}\Omega_R{}^2\left(x^2 + y^2\right) - \frac{(1-\mu)(1-\beta)}{\left((x+\mu)^2 + y^2 + z^2\right)^{1/2}} - \frac{\mu}{\left((x+\mu-1)^2 + y^2 + z^2\right)^{1/2}} \quad (4)$$

$$T = \frac{1}{2}\left(\dot{x}^2 + \dot{y}^2 + \dot{z}^2\right)$$

For the case of dust particles ejected from the surface, it is possible to calculate zero velocity curves (corresponding to C=2U) that are dependant on the lightness number β. Figure 2 represents those zero velocity curves for different particle sizes ejected with a fixed velocity of 10.34 m/s from a hypothetical 10 km radius asteroid at 1 AU from the Sun, and a set of example

trajectories for a particular ejection site on the equator at that same ejection velocity. The asteroid is assumed to be rotating with a 4 hour period around the *z*-axis, and the ejection velocity direction is selected radially outwards, normal to the asteroid surface. The asteroid density is assumed equal to the average NEO density[9] of 2.6 g/cm^3, while estimates on the particle radius are provided assuming spherical grains of constant density of 3.2 g/cm^3, representing a relatively low density olivine. If the composition and structure of the asteroid is uniform that would imply a macroporosity of 19%, close to the average S-type.[10]

Two values of β are particularly relevant: the β for which the zero velocity curves open ($5\text{x}10^{-3}$ in this particular case), which sets an upper bound in particle size for dust to escape, and the value of β that ensures a re-impact before one revolution.

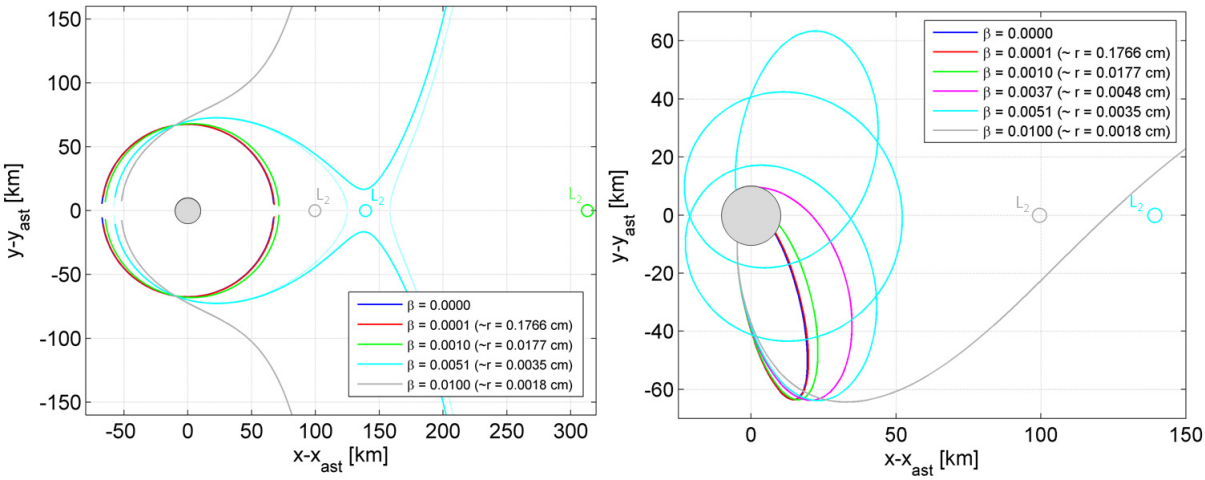

Figure 2. Zero velocity curves (left) and trajectories in the co-rotating frame (right) for ejection velocities of 10.34 m/s from a 10 km asteroid with a 4 hour rotational period, for different values of β. Particle size estimation are given assuming spherical grains of constant density and Q=1. Zero velocity curves are open for all particles with β larger than 0.0051 (cyan line). All particles with β lower than 0.0037 re-impact before one revolution for this particular ejection site (magenta line).

The first value sets a theoretical limit for the particles to escape, based solely on energy considerations. However, this provides little or no information if we want to predict when a particle would escape or not, as it depends not only on the energy level, but also the solar longitude of the ejection site and the orbital geometry in general. In fact, it is straightforward to calculate the positions in the *x*-axis of the two collinear libration points of the Sun-asteroid system using Eq. (5), and from there obtain the associated value of the integral of motion.

$$x_1 - \frac{(1-\mu)(1-\beta)}{(x_1+\mu)^2} + \frac{\mu}{(x_1+\mu-1)^2} = 0 \qquad C_1 = 2U(x_1)$$
$$x_2 - \frac{(1-\mu)(1-\beta)}{(x_2+\mu)^2} - \frac{\mu}{(x_2+\mu-1)^2} = 0 \qquad C_2 = 2U(x_2) \tag{5}$$

Substituting these values in Eq. (4) for the points on the surface of the asteroid, the ejection velocity required for the zero velocity curves to be open through the L_1 or L_2 points can be obtained. Because of the influence of the SRP perturbation, it is the L_2 point that offers the lowest energy, and thus also the lowest ejection velocity for escape trajectories of the dust grains, for the zero velocity curves to be open. The main effect of SRP on the location of the Lagrangian points

is to pull both the L_1 and L_2 points towards the Sun, resulting in an L_2 point closer to the surface of the asteroid (see Figure 2). Theoretically there is a particle size in which the L_2 point would be on the surface of the asteroid, and any particles of that size or smaller lifted from the surface with an infinitesimally small velocity at the correct time in a rotational period of the asteroid may escape. In reality, that region is normally in eclipse and the SRP would only affect particles that are still orbiting when the Sun comes into view.

It is then possible to calculate a guaranteed return velocity, for a given value of β, that ensures closed zero velocity curves and eventual re-impact with the surface. Figure 3 plots this velocity for a 10 km asteroid rotating along the z-axis assuming vertical ejection from the asteroid along the equator, where the rotation of the asteroid provides the largest contribution to the total kinetic energy, and thus an easier escape at lower velocities. This guaranteed return velocity shows small variations with the ejection site.

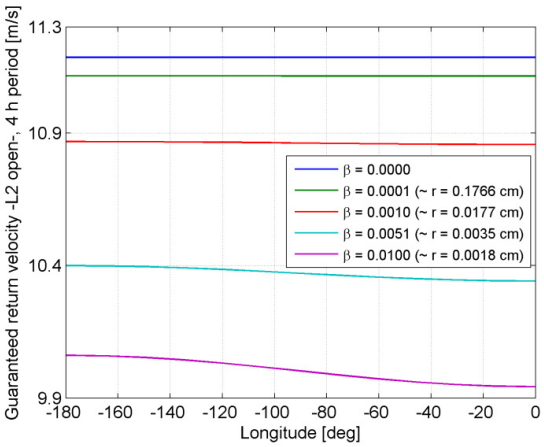

Figure 3. Guaranteed return velocity for dust particles ejected radially outwards along the equator of a 10 km asteroid with a 4 hour rotational period, for different values of β. The longitude of the ejection site is measured along the equator with respect to the antisolar direction.

On the other hand, the value of β that ensures re-impact before one revolution is highly dependent on the point of ejection, and the relative geometry of the orbit with respect to the Sun. Certain ejection sites will have all particles directly re-impact under the perturbation of solar radiation pressure, while others will have a limiting β that allows multiple revolutions. Figure 4 represents the re-impact time in a longitude-latitude grid of the ejection site for a β value of 0.0045 and a vertical ejection velocity of 10.34 m/s. The velocity was selected as the previously calculated mean guaranteed return velocity for the equator for that value of β. The figure on the right gives the re-impact time in number of periods calculated with the initial osculating semi-major axis at ejection. This semi-major axis, and thus period, are larger at the equator. For most of the surface of the asteroid the re-impact time is less than one initial period, while there is a region in the longitude's third quadrant that allows multiple revolutions. As expected, it is the region near the equator that has the highest probability of generating ejecta that perform more than one revolution. Also, the longitude's first and second quadrant, where the SRP acts against the velocity reducing the pericentre height, have shorter re-impact times that the third and fourth quadrant where the effect of the SRP perturbation raises the pericentre height.

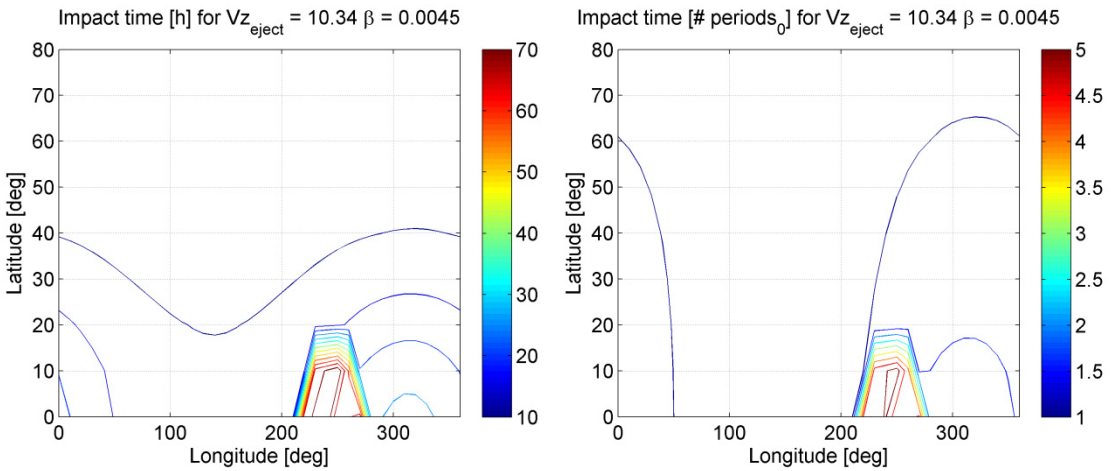

Figure 4. Re-impact time on a 10 km asteroid with a 4 hour rotational period, for dust particles of β = 0.0045 ejected radially outwards with 10.34 m/s ejection velocity. The re-impact time is given in hours (left) and number of initial periods (right).

It is difficult to draw more significant conclusions from this general form of the equations of motion, or to predict the re-impact of the dust without full numerical propagation. For this reason, a semi-analytical approximation is used in this paper to study the behaviour and various regimes of ejected dust around an asteroid.

HAMILTONIAN APPROACH

If we plot the previously generated trajectories in an eccentricity-ϕ plot, with the solar phase angle ϕ given by the following relation (see Figure 5 -left-):

$$\phi = \Omega + \arctan\left(\frac{\cos i \sin \omega}{\cos \omega}\right) - \lambda_{SUN} + \pi \tag{6}$$

where Ω represents the right ascension of the ascending node of the orbit of the dust particle around the asteroid, i and ω are the inclination and argument of the pericentre, and λ_{SUN} is the solar longitude, we obtain the plot in Figure 6. It can be immediately appreciated that the eccentricity increases for all trajectories with ϕ larger than 180 degrees, and decreases in the cases where ϕ is between zero and 180 degrees. Only a few trajectories with initial ϕ around 90 degrees and latitudes close to the equator perform multiple revolutions.

This plot resembles the phase space graphs in the work by Oyama et al.[11] for the limiting case with infinite SRP-gravity ratio. Their analysis was based on an approach proposed by Hamilton and Krikov[12] to study the behaviour of circumplanetary dust in a planar case, which consisted in orbit-averaging Lagrange's planetary equations over one revolution. This method was later used by Oyama and various authors to describe applications for high-area-to-mass ratio spacecraft for Earth geo-magnetic tail exploration,[11, 13] passive de-orbiting, and heliotropic orbits applications.[14] We will show that it is also well-suited to describe the trajectories followed by particles around asteroids under certain assumptions.

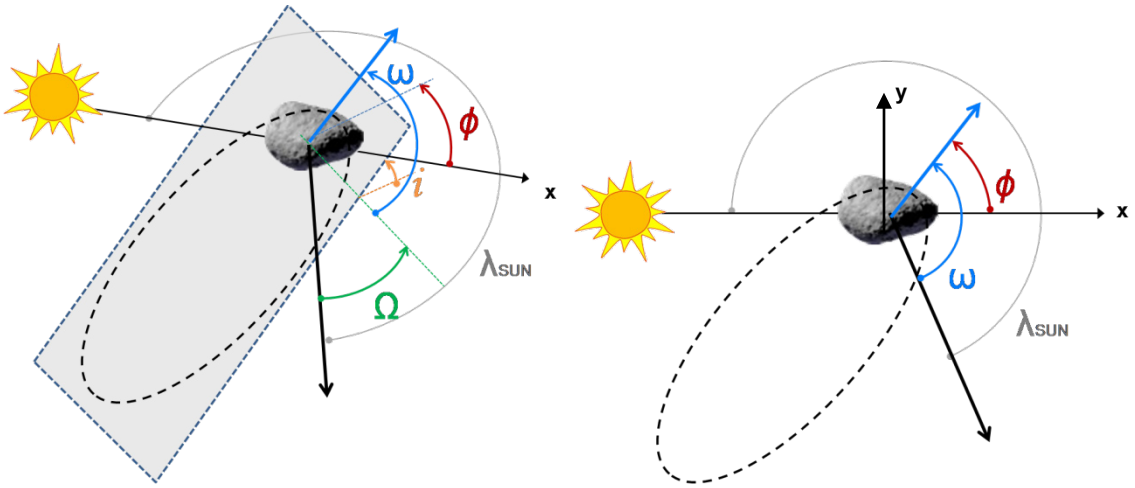

Figure 5. Definition of ϕ in the 3D case (left) and the planar case (right).

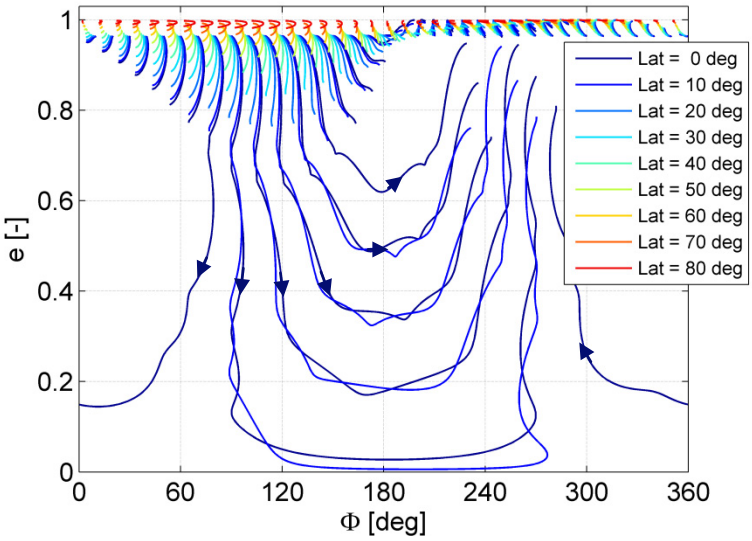

Figure 6. Eccentricity-ϕ plot of dust trajectories for different latitude-longitude ejection sites on a 10 km asteroid with a 4 hour rotational period, for dust particles of β = 0.0045 ejected radially outwards with 10.34 m/s ejection velocity.

Following loosely Hamilton and Krikov's methodology, we assume a planar case (see Figure 5 -right-) in which the rotation axis of the asteroid is perpendicular to the plane of movement of both the asteroid around the Sun and the dust particle around the asteroid. The angle ϕ between the anti-solar direction and the periapsis line is in the planar case simply given by $\phi = \omega - \lambda_{SUN} + \pi$. The dynamics of the dust under the influence of the solar radiation pressure perturbation and tidal forces caused by solar gravity can be described by the Hamiltonian:[12]

$$H = \sqrt{1-\bar{e}^2} + \frac{1}{2} A\bar{e}^2 \left(1 + 5\cos(2\phi)\right) - C\bar{e}\cos\phi \tag{7}$$

where the coefficients C and A correspond to the SRP and tidal term respectively, and can be expressed with the nomenclature followed by this paper as:

$$C = \frac{3}{2}\beta\sqrt{\frac{\mu_S}{\mu_A}\frac{\overline{a}}{d}} \qquad A = \frac{3}{4}\sqrt{\frac{\mu_S}{\mu_A}\frac{\overline{a}^3}{d^3}} \tag{8}$$

The eccentricity and semi-major axis that appear in Eq. (7) and Eq. (8) are orbit averaged values. This does not introduce large errors in the case of circumplanetary dust, as the variation of the semi-major axis over one revolution is zero[12] and the eccentricity changes slowly. In the case of dust around asteroids, the excursions of the osculating semi-major axis from the mean and the variations in eccentricity in one revolution are much larger, introducing errors in the analytical approximation, but we will show that the behaviour of the system is still well described with the Hamiltonian approach. The evolution of the eccentricity and angle ϕ is then given by the following Hamiltonian system in non-canonical form, which uses the solar longitude as its independent variable.

$$\begin{cases} \dfrac{\partial\overline{e}}{\partial\lambda_{SUN}} = -\dfrac{\sqrt{1-\overline{e}^2}}{\overline{e}}\dfrac{\partial H}{\partial\phi} \\ \dfrac{\partial\phi}{\partial\lambda_{SUN}} = \dfrac{\sqrt{1-\overline{e}^2}}{\overline{e}}\dfrac{\partial H}{\partial\overline{e}} \end{cases} \tag{9}$$

While the initial argument of pericentre of the ejected dust can be arbitrarily chosen by selecting an ejection site/time, the rest of the initial osculating orbital elements a_0, e_0 and true anomaly ν_0 of the ejected particles can be calculated as:

$$\begin{aligned} a_0 &= \frac{R}{2-\dfrac{R}{\mu_A}\left(v_{EJECT}{}^2+\left(\dfrac{2\pi}{T_A}R\right)^2\right)} \\ e_0 &= \sqrt{\left(v_{EJECT}\frac{2\pi}{T_A}R^2\right)^2+\left(\frac{4\pi^2}{T_A{}^2}R^3-\mu_A\right)^2}\Bigg/\mu_A \\ \nu_0 &= \arccos\left(\frac{\dfrac{4\pi^2}{T_A{}^2}R^3-\mu_A}{e_0\mu_A}\right) \end{aligned} \tag{10}$$

with R being the asteroid radius, T_A its rotational period and v_{EJECT} the ejection velocity, again assumed normal to the surface of the asteroid.

Figure 7 plots the comparison between the numerical propagation of the trajectories of ejected dust, and the isolines of constant Hamiltonian that the orbit-averaged elements should follow in the analytical approximation. The ejection velocity of this particular plot is 9.5 m/s and the rotation period of the asteroid 3 hours. No equilibrium points are found in the phase-space, due to the

high SRP perturbation when compared to the cases studied by Oyama[11] and Colombo.[14] Still, the Hamiltonian approach correctly predicts the increase in eccentricity for all points with $\phi > \pi$, resulting in a decrease in pericentre height and immediate re-impact before one revolution of all particles ejected in two full quadrants of the asteroid. The region close to $\phi = \pi / 2$ (which corresponds to ejection points with negative y in the third quadrant of longitude as foreseen in Figure 4) contains both trajectories that re-impact and others that perform multiple revolutions. The eccentricity is decreasing in all cases, but only in some does the pericentre height raise above the asteroid radius.

A series of operational guidelines can then already be drawn from these results with regards to the selection of the extraction site, to determine the solar longitudes when operations are safer to avoid re-impact of dust on crewed missions or equipment, and the maximum forces to be used when extracting material to avoid multi-revolution orbiting or escape of dust particles. If transient dust atmospheres are to be avoided, solar longitudes close to $\phi = -\pi / 2$ would be preferred. Operations at other solar longitudes are still feasible if the forces used ensure the ejection velocity of dust stays well below the limit that allows multi-revolution trajectories.

To better understand the multi-revolution regime, we plot the blue dashed horizontal line in Figure 7, which represents a critical eccentricity given by:

$$e_{CRIT} = 1 - \frac{R}{a_0} \tag{11}$$

The apocentres and pericentres in the numerical trajectories have been indicated with X and O markers. It can be observed that whenever the eccentricity is lower than the critical one by the first pericentre, the dust particle manages to perform multiple revolutions, until after a few loops the eccentricity grows again above the critical one. The maximum decrease in eccentricity over one revolution does not take place though exactly at $\phi = \pi / 2$, and the region of multi-revolution ejecta is thus not centred around it but shifted to the right on the plot.

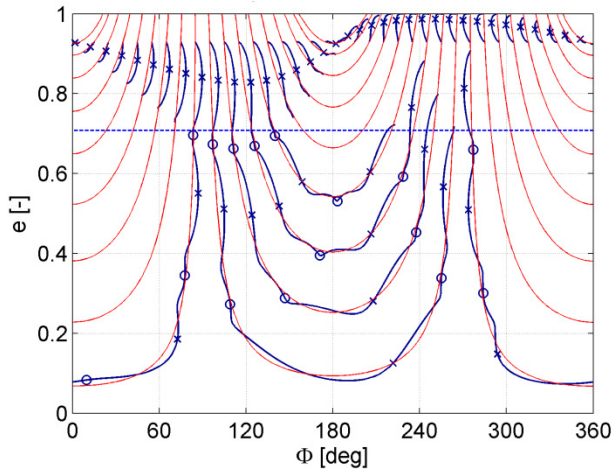

Figure 7. Isolines of constant Hamiltonian (red) and numerical propagation of ejected dust (dark blue) plotted in the eccentricity-ϕ phase space. Apocentres and pericentres of the numerical trajectories are indicated with X and O respectively.

Time integration

The Hamiltonian system in Eq. (7) can be transformed in full canonical form with the change of variable:[12]

$$k = \sqrt{1-\bar{e}^2} \tag{12}$$

resulting in:

$$\begin{cases} \dfrac{\partial k}{\partial \lambda_{SUN}} = \dfrac{\partial H}{\partial \phi} \\ \dfrac{\partial \phi}{\partial \lambda_{SUN}} = -\dfrac{\partial H}{\partial k} \end{cases} \tag{13}$$

It can be demonstrated that the tidal term A is only of the same order as the SRP for distances of the order of the 20 asteroid radii, while the trajectories we are interested in stay bounded well below this distance. If we thus neglect the tidal term A, Oyama et al.[11] showed that it is possible to integrate the system to obtain the time needed for a particle to travel along a line of constant Hamiltonian H^* between two values of k (or eccentricity), obtaining:

$$t - t_0 = \frac{-1}{\sqrt{\dfrac{d^3}{\mu_s}\left(1+C^2\right)}}\left(\arccos\frac{\left(1+C^2\right)k - H^*}{C\sqrt{1+C^2-H^*}} - \arccos\frac{\left(1+C^2\right)k_0 - H^*}{C\sqrt{1+C^2-H^*}} \right) \tag{14}$$

It is possible then to plot isolines of transfer time on the phase-space graphs, in particular we are interested in the isolines corresponding to the time until apocentre or pericentre, to determine if the next pericentre takes place before or after critical eccentricity is reached.

The period of the dust orbit around the asteroid is however affected by the SRP and depends greatly on the relative geometry with respect to the Sun. Integrating the Lagrange planetary equation for the semi-major axis assuming constant mean eccentricity, we obtain the evolution of a along the orbit:

$$a = a_0 \sqrt{\frac{1}{1 - 4\beta \dfrac{\mu_S}{\mu_A}\dfrac{a_0^{\,2}}{d^2}\dfrac{(1-\bar{e}^2)}{\bar{e}}\left(-\dfrac{\cos\phi + \bar{e}\sin\phi\sin\nu}{1+\bar{e}\cos\nu} + \dfrac{\cos\phi + \bar{e}\sin\phi\sin\nu_0}{1+\bar{e}\cos\nu_0} \right)}} \tag{15}$$

Integrating and averaging over one revolution and retaining only the first order terms on β, the mean semi-major axis can be approximated as:

$$\bar{a} \approx a_0 \left(1 + 2\beta \frac{\mu_S}{\mu_A}\frac{a_0^{\,2}}{d^2}\frac{(1-\bar{e}^2)}{\bar{e}}\left(-\frac{\cos\phi\sqrt{\dfrac{2}{1+\bar{e}}-1}}{1-\bar{e}} + \frac{\cos\phi + \bar{e}\sin\phi\sin\nu_0}{1+\bar{e}\cos\nu_0} \right) \right) \tag{16}$$

To obtain the orbital period it is also necessary to take into account the variation in argument of pericentre due to SRP. The Lagrange planetary equation for the derivative of time with respect to true anomaly, which includes a term related to the variation in ω is:

$$\frac{dt}{d\nu}=\sqrt{\frac{a^3}{\mu_A}}\frac{(1-e^2)^{3/2}}{(1+e\cos\nu)^2}\left[1-\beta\frac{\mu_S}{\mu_A}\frac{a^2}{d^2}\frac{(1-e^2)^2}{e(1+e\cos\nu)^2}\left(\cos\phi+\frac{\sin(\nu)\sin(\phi+\nu)}{1+e\cos\nu}\right)\right] \tag{17}$$

Integrating over one revolution considering the mean values of semi-major axis and eccentricities, the orbital period can be approximated as:

$$T\approx 2\pi\sqrt{\frac{\overline{a}^3}{\mu_A}}\left(1-\frac{1}{2}\beta\frac{\mu_S}{\mu_A}\frac{\overline{a}^2}{d^2}\cos\phi\left(\frac{12+13\overline{e}^2}{4\overline{e}}\right)\right) \tag{18}$$

A similar approach can be followed to obtain the first semi-period until apocentre. Plotting on the phase space the isolines of Eq. (14) corresponding to the time from initial true anomaly to apocentre and pericentre calculated analytically (see Figure 8), we can observe that they are a good match for the apsis points calculated with the numerical propagation. This allows an accurate prediction of when a particle is going to perform multiple revolutions. The region in the phase space where the isolines of time to pericentre is below the critical eccentricity line corresponds to multi-revolution trajectories. It is important to note that the critical eccentricity varies with the semi-major axis along the orbit, so there can be pericentres close to the limit that may impact or fly-over depending on the value of the semi-major axis at the re-impact time.

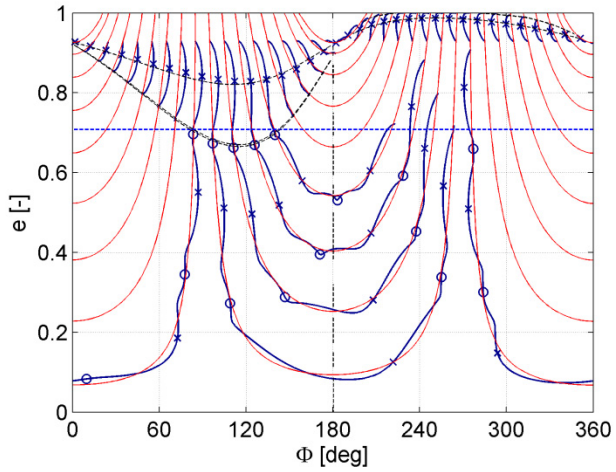

Figure 8. Apocentre and pericentre analytical time estimation on the eccentricity-ϕ phase space.

MATERIAL SORTING APPLICATIONS

One of the benefits of the differential effect of solar radiation pressure on ejected dust particles is the possibility to engineer these forces in order to passively separate material as a function of β. This processing of material can be considered either for separation of the same material as a function of the grain size on an asteroid of uniform composition (the larger the grain the lower the β), or alternatively, after a grinding process to reduce all materials to a similar grain size, as a method of separation of two materials with different density (again the higher the density of the material the lower the β). This concept is analogous to the process of winnowing in agriculture on Earth, used since thousands of years for separating grain from chaff due to differential atmospheric drag for materials with different area-to-mass ratio. Other methods such as separation by sedimentation or gravity tables are of common use in today's industrial world. The SRP sorting concept takes advantage of the low gravity on asteroids, which would render some of the other separation processes unfeasible (such as the use of a gravity table).

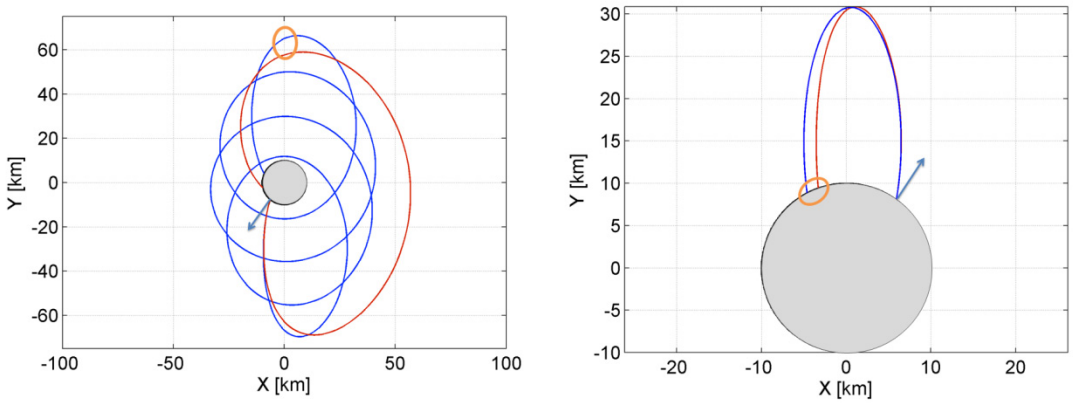

Figure 9. Schematic representation of separation strategies with a hovering spacecraft collection point (left) and a ground-based collection point (right). X-Y axes are parallel to the co-rotating frame axes and centred on the asteroid.

Two possible strategies for collecting the separated material can be devised (see Figure 9): a hovering spacecraft that collects on-orbit the material that has been lifted from the surface by a surface element or rover, or several collection points on ground at pre-calculated distances. Each method has preferred ejection points on opposite side of the asteroid ($\phi = \pm\pi/2$). The surface element can then collect material and, if needed, grind it for one asteroid revolution, and then eject it at the appropriate time depending on the selected strategy.

In the first method, the preferred ejection point is close to $\phi = \pi/2$, where the SRP has the effect of increasing the pericentre height and multiple revolutions are possible. The collection point should be hovering at a certain distance on the Y-axis. Once an ejection velocity has been selected, there is a minimum value of β that will avoid re-impact in the first revolution, essentially discriminating a maximum size of the grains of interest (larger grains would fall back onto the asteroid). The rest of the material would travel following isolines of constant H until eventually reaching the desired height on the Y-axis for collection. Figure 10 shows on an eccentricity-ϕ phase plot the lines that correspond to a particular height over the Y-axis on the asteroid assuming a constant mean semi-major axis. Only certain ejection sites close to $\phi = \pi/2$ can reach heights over 55 km on the Y-axis.

The passive separation takes place in time, as larger particles (particles with smaller β) require more revolutions and thus longer times to reach the collection area. This is shown in Figure 11 (left), where the time to come back to the initial eccentricity levels increases with decreasing β. The plot shows the time evolution of the eccentricity for different values of β and the same ejection site at the equator and $\phi = \pi/2$, a rotation period of 4 hours, and an ejection velocity of 10.34 m/s. Particles with $\beta \leq 0.004$ re-impact before the first pericentre.

It is possible to analytically estimate the time until collection by calculating with Eq. (14) the time required to reach the eccentricity of intersection of the ejection point isoline with $\phi = \pi$ or $\phi = 0$. Obtaining the intersection point is straightforward by substituting the phase angle ϕ in Eq. (7). Figure 11 right shows a comparison between the analytical estimates and the numerical propagated trajectories of the figure in the left. The collection point for each β is assumed as the point when the eccentricity reaches the value at the first apocentre again, and is indicated with markers in the left figure.

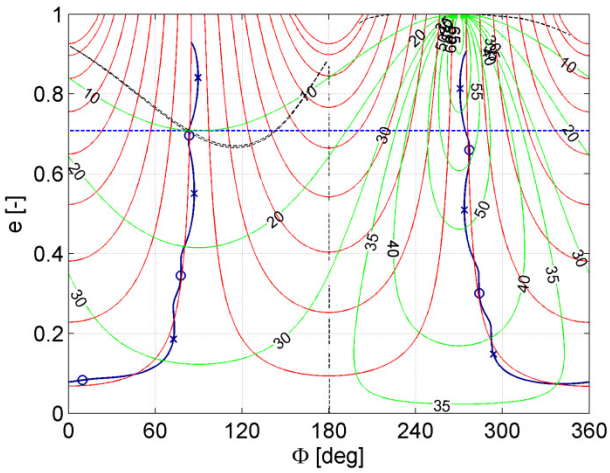

Figure 10. Eccentricity-ϕ phase space graph with isolines of constant height (green) over the Y-axis.

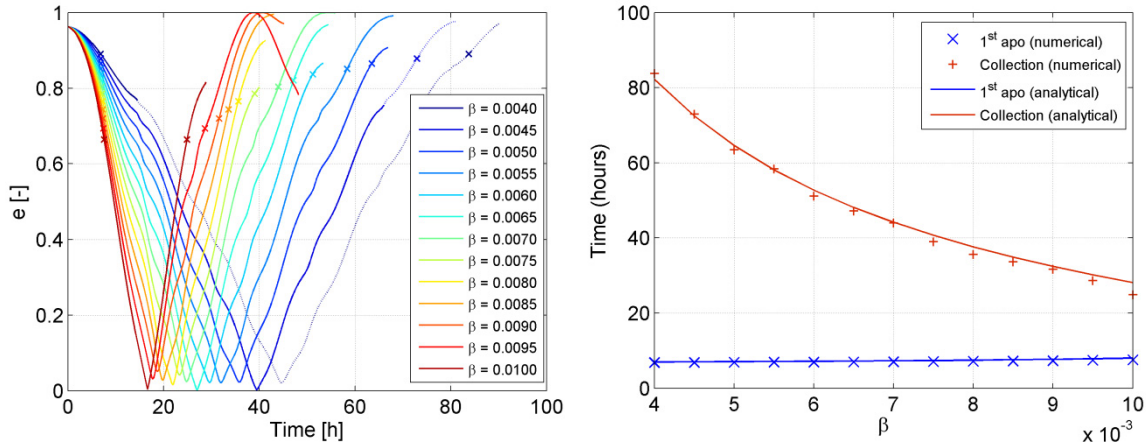

Figure 11. Left: Evolution of the eccentricity with time for $\phi = \pi/2$ and different values of β. Markers indicate the first apocentre and collection point. Discontinuous lines indicate there has been a re-impact on the surface. Right: Time to collection and analytical approximation as a function of β.

The main difficulty concerning this strategy is the large variation in height at the Y-axis crossing for orbiting particles of different β. Furthermore, simplifications in the model, such as the omission of the eclipse times and not including other perturbations such as high order gravitational terms, make the predictions in time much less accurate and the dispersion at the collection point higher. A non-planar case would have the added difficulty of the evolution of the orbital plane. Very large collectors (of the order of hundreds of meters for an asteroid of radius 10 km) would be required in order to capture a significant number of particles, or an elaborated station keeping strategy that changes height with time would be needed in order to compensate these variations. This greatly increases the complexity of operations for a hypothetical collection on-orbit. The ejection velocities required are also higher than for a ground based collection point.

The second method envisages a series of collector points spaced on the surface of the asteroid (or a collector band or strip extended over some distance). The differential separation of particles as a function of β is performed in space, rather than in time. The preferred ejection point is in this case close to or equal to $\phi = -\pi/2$ (pericentre on the negative Y-axis), which corresponds to tra-

jectories where the SRP reduces the pericentre height and thus re-impact is assured before one revolution for most values of β.

Figure 12 shows the distance between re-impact points for two regolith particles of different sizes and densities as a function of the ejection velocity. The ejection velocity in the X-axis has been scaled with the radius of the asteroid. For asteroids in the size range of 100 m to 10 km the required ejection velocities for the same separation densities scale well with the radius. Only in the case of fast rotators (blue lines with 2.5 hour period) if we increase the ejection velocity there is actually a bifurcation between the separation at a 1 km asteroid (dashed) and the 10 km one (continuous line), and there can even be cases with particles escaping. For a smaller 100 m asteroid the bifurcation takes place before but in all cases well above the 1 m separation horizontal line.

Figure 12 left assumes spherical particles of constant average density of 3.2 g/cm^3 (homogeneous asteroid of a low density olivine) for the suggested ejection site and different rotational periods of the asteroid. If the desired separation between two such particles of size 1 mm and 1 cm is 1 m, the graph shows that for an asteroid rotating with a 2.5 hour period the required ejection velocity would be 2 m/s on a 10 km asteroid, while this velocity would more than double in the case of a non-rotating asteroid (~ 4.5 m/s). If the size of the particles required for separation is one order of magnitude lower (0.1 mm and 1 mm), the ejection velocities range from 0.5 to 1.7 m/s for the same separation distance. These velocities are almost one order of magnitude lower than the ones suggested for a hovering spacecraft collection point.

The figure on the right assumes instead a differentiated asteroid with two materials to be separated. The regolith is assumed to have been previously grinded to grains of the same size (1 mm or 0.1 mm). Assuming 1 mm grains composed of plagioclase (average density of 2.68 g/cm^3) and a denser olivine or pyroxene (3.74 g/cm^3), the ejection velocities required for a 1 m separation on a 10 km asteroid range from 4 to 6.2 m/s depending on its rotation rate. For finely grinded 0.1 mm particles, these velocities are reduced to 1 to 2.6 m/s. As the required ejection velocities scale with the radius, on a 1 km size asteroid they would be one order of magnitude lower.

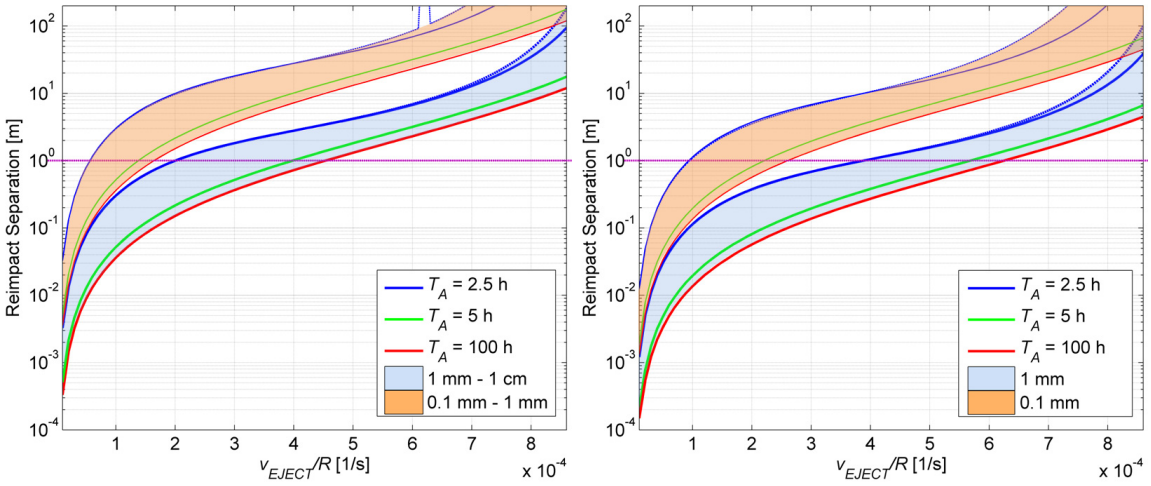

Figure 12. Re-impact point separation between 1 mm-1 cm (blue) and 0.1 mm-1 mm (orange) grains of homogenous density of 3.2 g/cm^3 (left figure); and between grains of different densities (2.68 and 3.74 g/cm^3) of the same size (1 mm in blue, 0.1 mm in orange, right figure). Particles are ejected with a phase angle ϕ of 90 degrees for different asteroid rotation periods.

Besides the lower ejection velocities required, other benefits of the ground base collection when compared to on-orbit collection is that eclipses have little or no influence in the trajectories of the particles as the preferred ejection sites result in eclipse-free trajectories. Other perturbations, such as higher order harmonics of the gravity field for the usually irregularly shaped asteroid would affect all particles in a similar form, regardless of the β value, so the differential effect of SRP would still cause a separation in re-impact points of the same order. Non-planar trajectories would be affected in a similar way over one revolution, and the only concern of an ejection point away from the equator would be a higher ejection speed required, similar to the case of a slowly rotating asteroid.

EFFECT OF UNCERTAINTIES

One of the concerns that arise when evaluating this method is the sensibility of the separation to errors or uncertainties in the ejection conditions. As the relative difference in grain size or density is small, errors in the velocity at ejection may induce greater dispersion on the grains than the solar radiation pressure perturbation.

The separation caused by velocity errors was calculated for various asteroid sizes and rotation periods. Figure 13 shows the re-impact point separation for an error in the velocity modulus of 1% (left) and an error in the ejection direction of 0.33 degrees (right). The colour patches indicating the separation by solar radiation pressure calculated in the previous section are superimposed for comparison. It can be easily observed that there is a limiting asteroid size for each ejection velocity for which the SRP induced separation is no longer effective compared to errors in velocity.

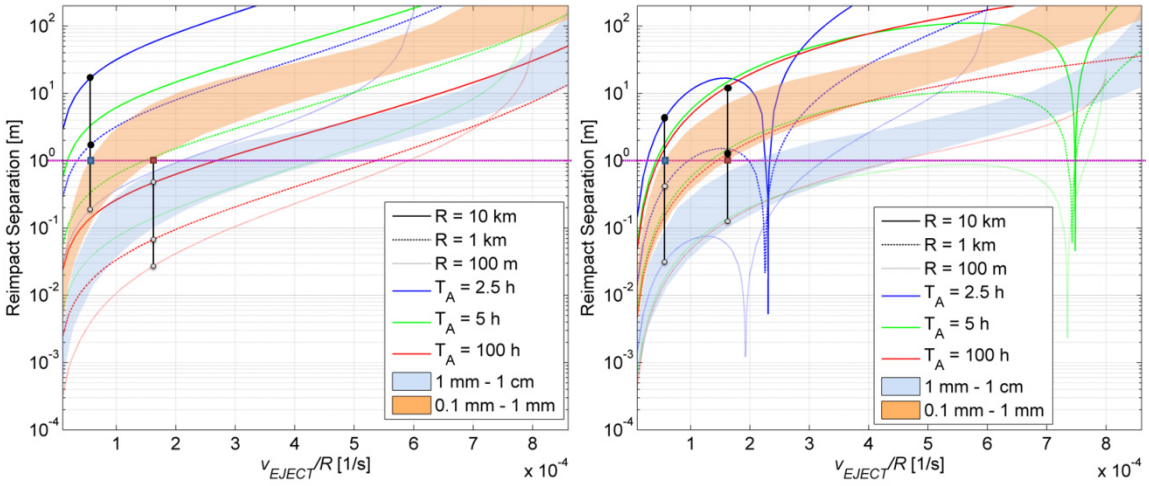

Figure 13. Re-impact point separation for errors in ejection velocity modulus of 1% (left figure) and errors in ejection angle (in-plane) of 0.33 degrees (right figure). Line-styles indicate asteroid size, while colours indicate its rotation period. The patches indicating the separation by differential SRP are also included for reference.

Focusing on specific examples (indicated by vertical lines), for the case of a fast rotating asteroid with a period of 2.5 h (blue square), the required ejection velocity for a separation of 1 m is equal to 0.06 x R^{15} m/s. With velocity modulus errors of 1%, the separation between equal particles would be of the order of 20 m for a 10 km asteroid, 2 m for a 1 km one, and 0.2 m for asteroids of 100 m radius. For a slowly rotating asteroid (period of 100 h), the separations due to errors in velocity modulus are of the order of 0.5, 0.07 and 0.02 for asteroids of 10, 1 and 0.1 km

radius respectively. While the dispersions in a slow rotator for asteroids up to 1 km seem acceptable for implementing the SRP particle sorting, they would render it useless for larger asteroids of 10 km radius, or for fast-rotators.

Figure 13 right shows a similar plot for errors in the velocity angle (only in-plane errors were considered). The separation induced by errors in angle has actually a minimum at a particular velocity, which lies close to the required ejection velocity to obtain an orbital period for the grains equal to the rotational period of the asteroid. Close to this velocity, an error in the ejection angle causes an error in semi-major axis that slightly modifies the re-impact time. As the particles perform a revolution at approximately the same time as the surface, there is a particular velocity for which errors in time would result in the same re-impact point at the surface, only slightly before or after in time. When considering the same two examples as in the previous case, the separation induced by errors in ejection angle is of the order of 4, 0.4 and 0.03 m for the fast-rotator case, and 10, 1 and 0.1 m for the slow-rotator. This seems to indicate that only asteroids of up to 100 m radius (or slightly larger) are good candidates for the sorting method proposed.

In order to have a more comprehensive analysis of the effect of additional uncertainties, such as in the size of the grains or the densities of the material, Monte Carlo simulations with 10000 shots were run for a 100 m radius fictitious asteroid rotating with a period of 5 h and with regolith that has previously been ground to a particle radius of 100 μm.

For the composition of the asteroid we assume an ordinary chondrite S-type asteroid containing mostly silicates (in general olivine-pyroxene with densities ranging from 3.2 to 4.37 g/cm^3) and a few traces of metal (of density 7.3 to 7.7 g/cm^3).[10] Table 1 lists the material composition as well as the assumed mean density and dispersion for 5 selected materials: Ni-Fe metallic grains, a high density orthopyroxene, two olivine silicates of medium and low density and a plagioclase silicate. The average grain density is of 3.52 g/cm^3 for this particular mix, which is well within the range of ordinary chondrites meteorites of L or H type.[16, 17]

Table 1. Regolith composition and densities.

Material	Percentage in regolith	Mean density (g/cm^3) [*, 10]	1-σ Std. dev. (g/cm^3)
Fe-Ni	2%	7.5	0.07
High density opx	15%	3.95	0.10
Medium density ol	50%	3.5	0.10
Low density ol	28%	3.2	0.05
Plagioclase	5%	2.68	0.04

Table 2 presents additional variables with uncertainties in the Monte Carlo simulation. The velocity modulus is selected to obtain a nominal separation of 1 m for an asteroid with a rotation period of 5 hours for 0.1 mm particles of the materials selected in the previous section (see Figure 13, right). The errors in velocity modulus follow a normal distribution with a 3-σ uncertainty of 3% of the velocity modulus. Errors in ejection angle are assumed in two orthogonal directions

[*] http://webmineral.com last accessed 29/01/2013

(along the longitude and latitude) with 1 deg 3-σ. The particles in the regolith are assumed to be ground prior to ejection down to a radius of 0.1 mm. The distribution of particle size is assumed to follow a lognormal distribution of parameters μ_{log} and σ_{log} of -9.21 and 0.05, which corresponds to a mode in particle size of 0.1 mm. The mean value is slightly higher and the standard deviation is approximately 5 μm, as can be seen in Table 2.

Table 2. Uncertainties in Monte Carlo simulation.

	Mean	1-σ Std. dev.
Velocity modulus (cm/s)	2.35	1%
Error angle (deg)	0	0.33
Particle radius (μm)	100.38	5.22

Figure 14 shows the result of one Monte Carlo run with 10000 shots. The upper left plot represents the trajectory in the Sun-asteroid co-rotating frame, with the Sun in the negative X-axis. Metallic particles are the least affected by the SRP and fall closer to the trajectory without perturbations (black line). In the lower left plot the same trajectories are plotted in a local horizontal frame with the *x*-axis representing the local displacement along the longitude lines on the asteroid. The Sun direction rotates but it is also close to the negative local *x*-axis due to the selected ejection point with $\phi = -\pi/2$. From the point of view of the ejector, the particles start travelling upwards along the local vertical up to a height of about 5 meters, and then start falling behind as the asteroid rotates, with the closest heavier particles falling around 3 m in the anti-solar direction and the lightest particle considered re-impacting 7 m away from ejection. A trajectory without SRP is also plotted (black line) for comparison. The re-impact points are represented on the two right plots of Figure 14. The upper graph shows the displacement along the local *x*-axis for different densities, while the lower one plots the re-impact point in the local horizontal frame, with *x* being the direction along the longitude lines, as in the other plots, and *y* along the latitude. The theoretical re-impact point without SRP is also indicated in both plots. The main effect of errors in velocity in the *y* direction is a displacement of the re-impact point in the *y* direction, not having much influence in the separation or mixing of particles.

The separation as a function of density is particularly effective for metallic particles, due to their well differentiated density. There is a much less clear separation among different silicate materials, although a gradient in density along the local *x*-axis is evident, from heavier pyroxene-olivine mixtures to lighter silicates of the plagioclase-feldspar family. The distances involved are also acceptable from an engineering point of view. A 10 meter collector band extended from the ejection module could be envisaged to collect material, or a rover could sweep the re-impact area in strips perpendicular to the *x* direction.

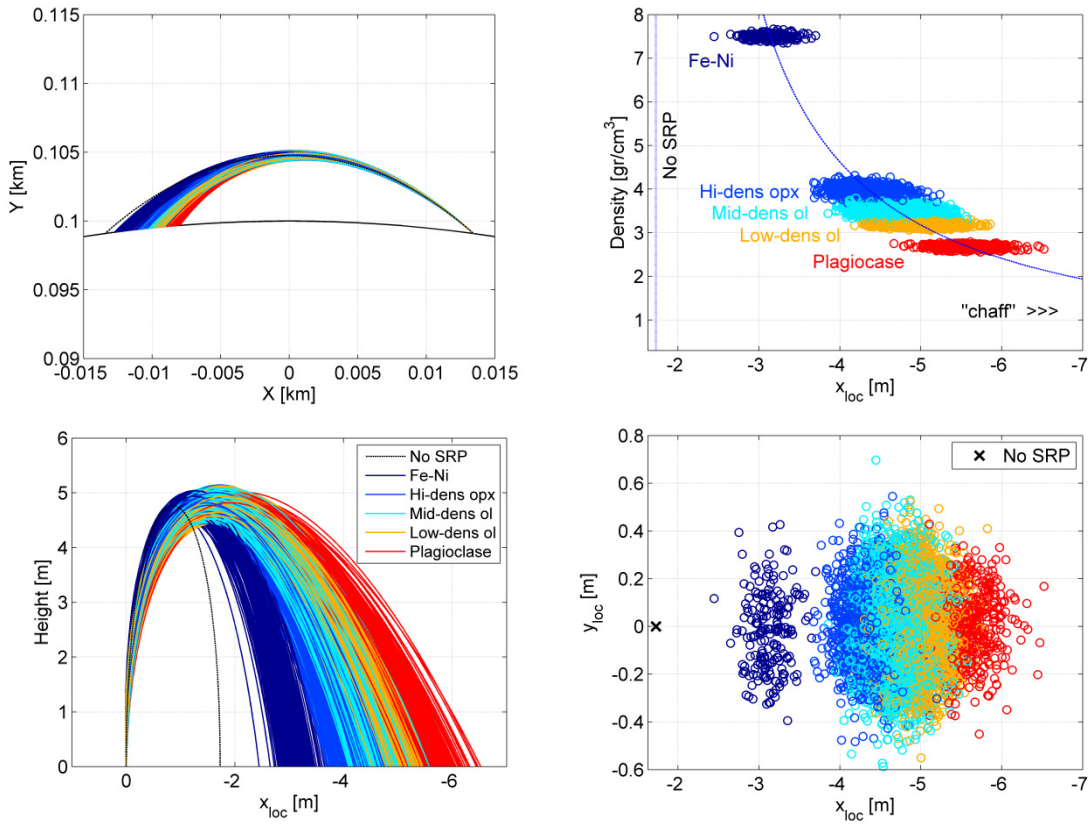

Figure 14. Monte Carlo run with 10000 ejected particles of different materials. Upper left plot shows trajectories in the Sun-asteroid co-rotating frame; lower left plots the height versus the local horizontal frame separation along the *x*-axis; upper right plot shows the separation as a function of density; the lower right graph shows the re-impact points in a local horizontal frame.

DISCUSSION AND MODELLING LIMITATIONS

The analysis presented so far represents a first order study on the feasibility of the concept of passive sorting of material by means of solar radiation pressure. This analysis already shows that ground based collection of material seems to be a promising technique. Nevertheless, further work on the numerical validation of these semi-analytical results will be required in order to ensure the efficacy of the method presented in a more complete dynamic model of a small body.

First, the use of the CR3BP for numerical propagation instead of a more complex model including the eccentricity of the asteroid orbit around the Sun has a minor influence on the results, as the timescales of the trajectories considered are short compared to the period of a NEO orbit around the Sun. In addition, the analytical results correspond to a simplified planar case and, although an extension to low inclination is possible and the general behaviour is not expected to change, a three-dimensional model is required for large inclination trajectories for ejecta from higher latitudes or from asteroids where the rotation axis is not perpendicular to the Sun-line. For these cases, the closed-form solution of the radiation pressure approximation (RPA) by Richter and Keller,[3] could allow analytically an extension of the problem to 3D. The RPA approach has already been used in the literature to study stable orbits of ejecta among small bodies.[18] It may

however not be best suited to study trajectories close to an asteroid, due to the averaging techniques used.

The irregular shape of asteroids would also have an important effect on the method proposed, not only due to the unmodeled gravitational perturbations that may render some of the multi-revolution trajectories presented unfeasible,[19, 20] but also due to the changes in the re-impact point position and direction as a function of the local geometry. Higher order gravitational terms should affect all particles independently of their lightness number, so their influence on the SRP induced separation is expected to be limited for the on-ground collection method where a full revolution does not take place, but the shape of the asteroid will change the departure are re-impact conditions greatly.

Regarding the solar radiation pressure force modelling and the material properties, the same reflectance was assumed for all materials by setting the radiation pressure scattering coefficient Q=1, corresponding to complete absorption. The lightness number β is proportional to Q/ρ and material dependant variations in the radiation pressure coefficient would affect the separation between particles. However, reflectance spectra analysis from meteorite metal-silicate mixtures[21] show that the absolute reflectance of orthopyroxene and olivine silicates is greater than that of denser metallic mixtures, thus having the effect of a greater gap in β values, and theoretically increasing the re-impact separation between metallic and silicate particles.

Finally, more complex models of particle cloud propagation may be required to take into account shading effects and collisions between particles.

CONCLUSIONS

The engineering of the solar radiation pressure perturbation is a promising method for separation of dust grains around small bodies. Simplified models to describe the behaviour of particles ejected at low velocities from an asteroid surface have been described and applied to a spherical rotating asteroid. The planar Hamiltonian approach and the phase space graphs introduced have proven to be useful tools to study and understand the behaviour of dust, and they allow predicting the conditions to perform multiple revolutions or to re-impact as a function of the ejection site and the size of the particle.

From these models, operational guidelines have been suggested regarding extraction site selection and safe ejection velocities to avoid the danger of transient dust atmospheres during scientific or mining operations on a small body. A novel passive SRP separation method has been proposed, including two variations of the collection strategy: on-orbit and on-ground. The analysis shows that the winnowing-like method with collection on ground can be an effective mechanism for material processing, while the on-orbit collection presents greater challenges.

ACKNOWLEDGEMENTS

The work reported in this paper was supported by European Research Council grant 227571 (VISIONSPACE). We would also like to acknowledge the financial support of the travel grants of the Royal Aeronautical Society for the attendance to the congress.

REFERENCES

[1] N.R. Augustine, et.al., Seeking a Human Spaceflight Program Worthy of a Great Nation, Review of U.S. Human Spaceflight Plans Committee, 2009.
[2] D.J. Scheeres, C.M. Hartzell, P. Sánchez, M. Swift, Scaling forces to asteroid surfaces: The role of cohesion, Icarus, 210 (2010).

[3] K. Richter, H.U. Keller, On the Stability of Dust Particle Orbits around Cometary Nuclei, Icarus, 114 (1995) 355-371.
[4] P. Michel, Physical properties of Near-Earth Objects that inform mitigation, Acta Astronautica, In Press (2012).
[5] D.J. Scheeres, D.D. Durda, P.E. Geissler, The Fate of Asteroid Ejecta, in: W. Bottke, A. Cellino, P. Paolicchi, R.P. Binzel (Eds.) Asteroids III, University of Arizona Press, Tucson, 2002, pp. 527-544.
[6] Y.A. Chernikov, The Photogravitational Restricted Three-body Problem, Soviet Astronomy - AJ, 13 (1970) 176-181.
[7] D.W. Schuerman, The restricted three-body problem including radiation pressure, The Astrophysical Journal, 238 (1980) 337-342.
[8] J.F.L. Simmons, A.J.C. McDonald, J.C. Brown, The restricted 3-body problem with radiation pressure, Celestial Mechanics, 35 (1985) 145-187.
[9] S.R. Chesley, P.W. Chodas, A. Milani, G.B. Valsecchi, D.K. Yeomans, Quantifying the Risk Posed by Potential Earth Impacts, Icarus, 159 (2002) 423-432.
[10] D.T. Britt, D. Yeomans, K. Housen, G. Consolmagno, Asteroid Density, Porosity, and Structure, in: W. Bottke, A. Cellino, P. Paolicchi, R.P. Binzel (Eds.) Asteroids III, University of Arizona Press, Tucson, 2002, pp. 485-500.
[11] T. Oyama, H. Yamakawa, Y. Omura, Orbital Dynamics of Solar Sails for Geomagnetic Tail Exploration, Journal of Spacecraft and Rockets, 45 (2008) 316-323.
[12] D.P. Hamilton, A.V. Krikov, Circumplanetary Dust Dynamics: Effects of Solar Gravity, Radiation Pressure, Planetary Oblateness, and Electromagnetism, Icarus, 123 (1996) 503-523.
[13] C. McInnes, M. Macdonald, V. Angelopolous, D. Alexander, Geosail: Exploring the Magnetosphere Using a Small Solar Sail, Journal of Spacecraft and Rockets, 38 (2001) 622-629.
[14] C. Colombo, C. Lücking, C.R. McInnes, Orbital dynamics of high area-to-mass ratio spacecraft under the influence of J2 and solar radiation pressure, in: 62nd International Astronautical Congress, Cape Town, South Africa, 2011.
[15] J. Hickman, The Political Economy of Very Large Space Projects, Journal of Evolution and Technology, 4 (1999).
[16] G.J. Flynn, L.B. Moore, W. Kl¨ock, Density and Porosity of Stone Meteorites: Implications for the Density, Porosity, Cratering, and Collisional Disruption of Asteroids, Icarus, 142 (1999) 97-105.
[17] G.J. Consolmagno, D.T. Brittb, R.J. Macke, The significance of meteorite density and porosity, Chemie der Erde, 68 (2008) 1-29.
[18] D.J. Scheeres, F. Marzari, Temporary orbital capture of ejecta from comets and asteroids: Applications to the Deep Impact experiment, Astronomy and Astrophysics, 356 (2000).
[19] D.J. Scheeres, S.J. Ostro, R.S. Hudson, R.A. Werner, Orbits Close to Asteroid 4769 Castalia, Icarus, 121 (1996) 67-87.
[20] D.J. Scheeres, S.J. Ostro, R.S. Hudson, E.M. DeJong, S. Suziki, Dynamics of Orbits Close to Asteroid 4179 Toutatis, Icarus, 132 (1998) 53-79.
[21] E.A. Cloutis, P.S. Hardersen, V. Reddy, M.J. Gaffey, D.T. Bailey, M.A. Craig, Metal-orthopyroxene and metal-olivine mixtures: spectral reflectance properties and implications for asteroid spectroscopy, in: 40th Lunar and Planetary Science Conference, The Woodlands, Texas, 2009.